Acta Scientific Veterinary Sciences (ISSN: 2582-3183)

Volume 7 Issue 11 November 2025

Research Article

Computational Structural Modelling, Characterization, and Interaction Analysis of *Nicotiana rustica* Roq1 and *Ralstonia solanacearum* XopQ Effector Proteins

Dishita Mishra[1,2#], Ranjit Shaw[3,4#], Kishori Lal[1#], Md Zishan Ansari[5] and Radha Chaube[3]*

[1]*School of Biotechnology, Institute of Science, Banaras Hindu University, Varanasi-221005, Uttar Pradesh, India*

[2]*Kusuma School of Biological Sciences, IIT Delhi, Hauz Khas, New Delhi-110016, India*

[3]*Department of Zoology, Institute of Science, Banaras Hindu University, Varanasi-221005, Uttar Pradesh, India*

[4]*Department of Biosciences and Bioengineering, IIT Bombay, Powai, Mumbai- 400076, India*

[5]*Department of Biological Sciences, Indian Institute of Science Education and Research (IISER), Berhampur760003, Odisha, India*

***Corresponding Author:** Radha Chaube, Department of Zoology, Institute of Science, Banaras Hindu University, Varanasi-221005, Uttar Pradesh, India.

# Equal Contributions.

Received: October 24, 2025

Published: November 13, 2025

Abstract

The interaction between plants and pathogens is a co-evolutionary process. Host plants have innate immunity receptors that recognize pathogen-related effector proteins. *Ralstonia solanacearum* causes bacterial wilt by secreting effector molecules via the type III secretion system. XopQ protein in this bacterium is recognized by the Roq1 receptor in Solanaceae species. However, the physico-chemical mechanism underlying this interaction in *Nicotiana rustica* is still not completely understood. In this study, we used a computational approach to identify and characterize the interaction between the *N. rustica* Roq1 and the *R. solanacearum* XopQ proteins. The primary sequence of Roq1 was predicted using FGENESH and functionally characterized using InterProScan. Physicochemical properties were analyzed using ProtParam. Homology modeling of Roq1 and XopQ was performed using SWISSMODEL, validated by SAVES v6.1, and classified using CATH. Molecular docking was performed using ZDOCK 3.0.2, and interaction hot spots were identified using the KFC Server. Molecular dynamics simulations using WebGro assessed structural stability. A total of 14 residues in Roq1 and 23 residues in XopQ were found to be actively involved in stable protein–protein interactions. The Roq1-XopQ complex exhibited enhanced stability, suggesting conformational changes associated with immune activation. The understanding of Roq1-XopQ interaction can be important in the modification of immune receptors through molecular breeding or genome editing. The identification of conserved interface residues can be useful for the transfer of Roq1-like resistance traits into crops susceptible to bacterial wilt and related diseases. Transgenic expression of Roq1 in crops like tomato and pepper confers strong immunity, minimizing yield losses and reducing pesticide reliance for sustainable agriculture. The *in-silico* findings reported in this study can be further validated by *in vivo* studies.

Keywords: Innate Immunity; Type III Secretion System; Physico-chemical Mechanism; Molecular Docking; Protein-Protein Interactions

Introduction

Plant-pathogen interaction is a complex and continuous co-evolutionary process. Bacterial wilt is a necrotic vascular disease caused by *Ralstonia solanacearum*, a Gram-negative phytopathogenic bacterium. This pathogen infects nearly 200 plant species, including several economically important crops such as banana, potato, pepper, tomato, and tobacco [1,2]. Typical symptoms of the disease include necrosis, vascular discoloration, wilting, and ultimately death of the plant [3]. Granville wilt in tobacco is one of the deadliest crop diseases that results in 15% to 35% yield losses worldwide [4]. *R. solanacearum* invades the host plant through wounds or vascular tissues in the root system. Once inside, it proliferates extensively to colonize the xylem vessels. As a result, xylem vessels are clogged, and water and nutrient transport to the aerial parts of the host plant is retarded [5]. Despite its severe impact on crop productivity globally, the physicochemical mechanism governing host-pathogen interactions during bacterial wilt remains incompletely understood. Plants possess an innate immune system that is able to recognize the invading pathogens. In response, virulent pathogens have evolved to secrete effector proteins that help them evade the initial defense barrier.

Nicotiana rustica, commonly known as strong tobacco, is a rainforest species belonging to the Solanaceae family. Compared to the widely cultivated *Nicotiana tabacum*, *N. rustica* is economically advantageous as it produces nearly nine times more nicotine, making it an important source for producing bio-pesticides [6]. However, *N. rustica* is highly susceptible to a variety of phytopathogens. *R. solanacearum* is a causative agent of bacterial wilt in *N. rustica*. It secretes numerous effector molecules through its type III secretion system (T3SS), which are required for manipulating host physiology and evading the immune system [7]. Among these, Xanthomonas outer protein Q (XopQ), first characterized in *Xanthomonas euvesicatoria,* is a highly conserved and widely distributed protein across several pathogenic species [8,9].

In the present study, we aim to identify the host receptor in *N. rustica* that interacts with the *R. solanacearum* XopQ effector protein, and to characterize the molecular features of this interaction using computational methods. The Roq1-XopQ interaction may initiate downstream immune signal pathways in the host that are yet to be completely understood. Although experimental methods such as X-ray crystallography and nuclear magnetic resonance (NMR) spectroscopy are highly accurate, they are often time-consuming and resource-intensive. As a more efficient approach, *in silico* homology modeling enables the prediction of the three-dimensional (3D) protein structures based on their amino acid sequences and known structures of homologous proteins [10,11]. According to this method, proteins with at least 30% sequence identity are likely to adopt similar 3D folds [12]. Following homology modeling, we performed molecular docking and molecular dynamics (MD) simulations to study the protein-protein interaction dynamics, stability, and the hot spot residues between XopQ and Roq1. This study lays the foundation for future *in vivo* validation of proposed *in silico* protein-protein interactions.

Literature Review

The immune response is organized into two major layers. The first is pathogen-associated molecular pattern (PAMP)-triggered immunity (PTI), initiated when pattern recognition receptors (PRRs) on the plasma membrane detect conserved PAMPs located on the pathogen surface [13]. Plants have co-evolved mechanisms to recognize these effector molecules using suitable receptors, and in turn activate effector-triggered immunity (ETI), which is the second line of defense. ETI results in a strong immune reaction. It is accompanied by a hypersensitive response, which causes localized cell death at the site of infection [14]. This prevents further spread of the pathogenic infection in the host tissues. A large proportion of ETI responses in plants are mediated by the nucleotide-binding leucine-rich repeat (NLR) superfamily of intracellular immune receptors [15]. The structure of NLR proteins enables them to perceive a wide range of microbial pathogens. These receptors are activated either through direct physical interactions with the effector protein or by indirect recognition through the detection of proteins that undergo modifications like acetylation, uridylation, or cleavage [16]. NLRs typically contain three domains, namely, a conserved central nucleotide-binding domain, a conserved oligomerization domain, and a C-terminal leucine-rich repeat (LRR). The two dis-

tinct N-terminal domains classify NLRs into two distinct subclasses. CC-NLRs (CNLs) possess a coiled-coil (CC) domain, while TIR-NLRs (TNLs) possess a Toll/interleukin-1 receptor (TIR) domain. Moreover, a third subclass called helper NLRs (hNLRs) has been identified. Although hNLRs do not directly bind pathogen effectors, they play a key role in transmitting immune signals that activate ETI responses [17]. Studies in *Nicotiana benthamiana* have demonstrated that a TIR-NLR receptor, Roq1, directly interacts with the surface residues and the predicted catalytic site of the effector XopQ. This promotes oligomerization of the Roq1 protein into a tetrameric resistosome [18] to activate ETI and promote localized cell death [19]. Recent findings indicate that *R. solanacearum* also secretes the XopQ effector protein and that a Roq1-like homolog exists in *N. rustica*, which is hypothesized to form a protein complex with the bacterial XopQ effector.

Materials and Methods

Identification of *N. rustica* Roq1 and *R. solanacearum* XopQ target proteins through comparative analysis

The amino acid sequences of the reference proteins *Xanthomonas euvesicatoria* XopQ (PDB ID: 7JLU) and *N. benthamiana* Roq1 (PDB ID: 7JLX) were obtained from the Protein Data Bank (PDB) (https://www.rcsb.org/). The whole genome shotgun sequence of *N. rustica* (NCBI ID: MDKG01103070.1) was retrieved from the National Center for Biotechnology Information (NCBI) database. The corresponding gene and amino acid sequences of the *N. rustica* Roq1 protein were predicted using the FGENESH server (http://www.softberry.com/berry.phtml?topic=fgenesh&group=programs&subgroup=gfind) [20].

The amino acid sequence of the *R. solanacearum* XopQ protein was obtained through the NCBI Basic Local Alignment Search Tool (NCBI-BLAST). Functional annotation of the *N. rustica* Roq1 sequence was carried out using the InterProScan web server (https://www.ebi.ac.uk/interpro/search/sequence/), which identified its domains, motifs, and other conserved functional features. For comparative analysis, the reference *N. benthamiana* Roq1 protein sequence was also analyzed using InterProScan to assess domain conservation and to identify putative active sites involved in effector recognition [21].

Physico-chemical characterization of *N. rustica* Roq1 and *R. solanacearum* XopQ target proteins

The physico-chemical characteristics of the target *N. rustica* Roq1 and *R. solanacearum* XopQ proteins were analyzed using the ProtParam tool available on the ExPASy server (https://web.expasy.org/protparam/), developed by the Swiss-Prot group [22]. The amino acid sequences of both target proteins were individually submitted to ProtParam to evaluate several parameters, including amino acid composition, molecular weight, theoretical isoelectric point (pI), and aliphatic index.

Structural prediction of *N. rustica* Roq1 and *R. solanacearum* XopQ proteins by homology modeling and CATH classification

As no experimentally determined 3D structures were available for *N. rustica* Roq1 and *R. solanacearum* XopQ proteins, their Fast-All (FASTA) sequences were individually submitted to the SWISS-MODEL server (https://swissmodel.expasy.org/) [23] to predict reliable 3D structures through template-based homology modeling. The quality and reliability of the predicted models were assessed using ERRAT, PROCHECK, and VERIFY 3D tools on the SAVES v6.1 server (https://saves.mbi.ucla.edu/) [24-28]. The validated PDB files were then visualized using BIOVIA Discovery Studio 2021 (https://www.3ds.com/products/biovia/discovery-studio) for detailed structural analysis [29]. Furthermore, the CATH database (https://www.CATHdb.info/) [30] was used for structural and functional classification based on parameters including class (C), architecture (A), Topology (T), and homologous superfamily (H).

Structural validation and quality assessment of the modeled 3D protein structures

The quality and reliability of the homology-modeled 3D structures of *N. rustica* Roq1 and *R. solanacearum* XopQ proteins were evaluated using the Qualitative Model Energy Analysis (QMEAN)

4.3.1 tool on the SWISS-MODEL web server [31], which estimates model quality at both the local and global levels. The predicted PDB files were further uploaded to the SAVES v6.1 server (https://saves.mbi.ucla.edu/), where the ERRAT, VERIFY 3D, and PROCHECK tools were employed for detailed structural validation. These tools examine stereochemical parameters and assess the compatibility of the 3D models with their corresponding amino acid sequences. PROCHECK provides detailed outputs for each stage of the quality assessment [22]. Various PostScript-formatted plots were generated to visualize the results. Ramachandran plot analysis was performed to evaluate dihedral angle distributions and the conformational fidelity of the protein backbone.

Protein-protein molecular docking

Automated molecular docking was carried out to predict potential binding conformations between target proteins XopQ and Roq1. Virtual screening of multiple compound libraries was performed to evaluate interactions and identify binding conformations [32,33]. The predicted 3D structures of the target proteins were submitted to the ZDOCK 3.0.2 server (https://zdock.umassmed.edu/) [34] to generate the XopQ-Roq1 protein-protein interaction complex.

Identification and characterization of binding hot spots at the protein-protein interface

The docked XopQ-Roq1 complex was submitted to the Knowledge-based FADE and Contacts (KFC) server (http://kfc.mitchell-lab.org/) [35,36] for the identification of protein-protein interaction hot spots and energetically favorable interface residues. The resulting complex was further analyzed using BIOVIA Discovery Studio 2021 (https://www.3ds.com/products/biovia/discovery-studio) to highlight and analyze key amino acid residues contributing to the interaction between the target proteins.

Comparative molecular dynamics simulation and conformational stability analysis

MD simulations were conducted using the WebGro server (https://simlab.uams.edu/) using the GROMACS simulation package [37] to evaluate the dynamic behavior, conformational flexibility, and stability of the target proteins during complex formation. The WebGro server implements a standard simulation workflow comprising pre-processing, minimization of energy, equilibration, molecular dynamics, and analysis of trajectory in an aqueous environment. The PDB files of each individual target protein and their docked complex were submitted for simulation, followed by structural preprocessing. Energy minimization was performed for 5000 steps using default parameters. The system was subsequently equilibrated under constant volume (NVT) and constant pressure (NPT), and MD simulation time was set at 50 nanoseconds (ns).

Results

Identification of *N. rustica* Roq1 and *R. solanacearum* XopQ target proteins through comparative analysis

The amino acid sequence of the *N. rustica* Roq1 protein was predicted using FGENESH [20], whereas the sequence of the *R. solanacearum* XopQ protein was retrieved using NCBI-BLAST. Both proteins were individually analyzed using the InterProScan web server to identify conserved domains and homologous functional sites through comparison with reference sequences [21]. The *N. rustica* Roq1 protein was identified as a functional homolog of the known *N. benthamiana* Roq1 protein. It was classified within the disease-resistance protein family (InterPro ID: IPR044974) and the leucine-rich repeat domain superfamily (InterPro ID: IPR032675) of plants. Its functional domains included the toll/interleukin-1 receptor (TIR) homology domain (InterPro ID: IPR000157), the NB-ARC domain (InterPro ID: IPR002182), and the C-terminal jelly roll/Ig-like domain (C-JID) (InterPro ID: IPR045344). The *R. solanacearum* XopQ protein was classified under the ribonucleoside hydrolase-like superfamily (GO:0016799).

Physico-chemical characterization of *N. rustica* Roq1 and *R. solanacearum* XopQ target proteins

Physico-chemical characterization using the ProtParam tool revealed that the *N. rustica* Roq1 protein consists of 1312 amino acids, with an estimated molecular weight of 151 kDa, and a theoretical isoelectric (pI) of 5.8. Analysis of its amino acid composition indicated that leucine, serine, glutamic acid, and lysine together account for approximately 40% of the residues. In contrast, the *R.*

solanacearum XopQ protein comprises 487 amino acids with an estimated molecular weight of 52.4 kDa and a theoretical pI of 6.4. Its amino acid composition showed that alanine, leucine, proline, valine, glycine, arginine, and asparagine are the most abundant residues, collectively accounting for more than 60% of the total residues, while cysteine, tryptophan, tyrosine, and methionine were the least abundant.

Structural prediction of *N. rustica* Roq1 and *R. solanacearum* XopQ proteins by homology modeling and CATH classification

Homology modeling of the target proteins using the SWISS-MODEL server generated reliable 3D structures. Visualization of the predicted 3D models with BIOVIA Discovery Studio 2021 [29] revealed the *R. solanacearum* XopQ protein predominantly adopts an alpha-helical configuration throughout most of its structure, whereas the *N. rustica* Roq1 protein exhibited complex domain architecture representative of typical plant immune receptor proteins (Figure 1).

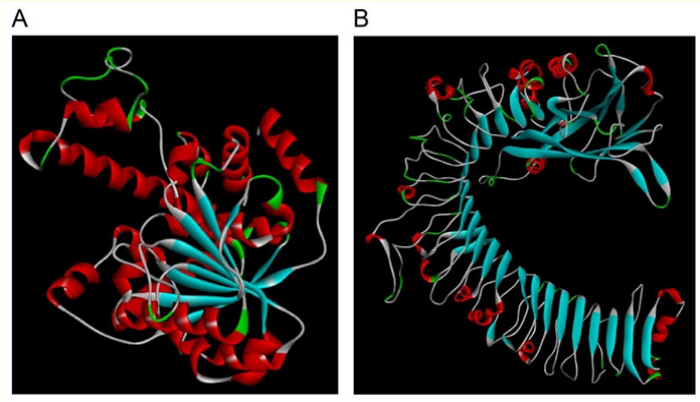

Figure 1: 3D structural models of the *R. solanacearum* XopQ and *N. rustica* Roq1 proteins generated by the SWISSMODEL server and visualized using BIOVIA Discovery Studio 2021. A) Predicted 3D structure of the *R. solanacearum* XopQ protein showing a predominant alpha-helical configuration across the majority of the protein. B) Predicted 3D structure of the *N. rustica* Roq1 protein displaying a complex domain architecture characteristic of typical plant immune receptor proteins.

The CATH database classifies protein domains based on their structural and functional characteristics, as well as sequence information. At the C-level, proteins are grouped into four categories according to secondary structure content as: 1) alpha, 2) beta, 3) alpha and beta, and 4) domains with minimal secondary structure. The A-level describes the overall three-dimensional arrangement of the structure. At the T-level, the connectivity and topology of the structure are considered, while the H-level evaluates evolutionary relationships to determine homologous sequences. The CATH classifications of the *R. solanacearum* XopQ and *N. rustica* Roq1 proteins are summarized in Table 1.

Protein	Source	Characters	C(Class)	A(Architecture)	T(Topography)	H(Homologous Superfamily)
XopQ	*Ralstonia solanacearum*	CATH ID	3	3.90	3.90.245	3.90.245.10
		Interpretation	αβ	αβ Complex	Inosine Uridine Nucleoside N-Ribohydrolase; Chain A	Ribonucleoside Hydrolase-like
Roq1	*Nicotiana rustica*	CATH ID	3	3.40	3.40.50	3.40.50.10140
		Interpretation	αβ	3-Layer (αβα) Sandwich	Rossmann Fold	Toll/Interleuki n-1-receptor homology (TIR) domain

Table 1: Hierarchical structural classification of the *R. solanacearum* XopQ and *N. rustica* Roq1 proteins according to the CATH database.

Structural validation and quality assessment of the modeled 3D protein structures

The quality assessment of the modeled *R. solanacearum* XopQ and *N. rustica* Roq1 protein structures using the QMEAN 4.3.1 tool is shown in Figure 2. The evaluation is based on QMEAN 4.3.1 scoring functions and global scores in comparison with the experimentally resolved structures in the PDB.

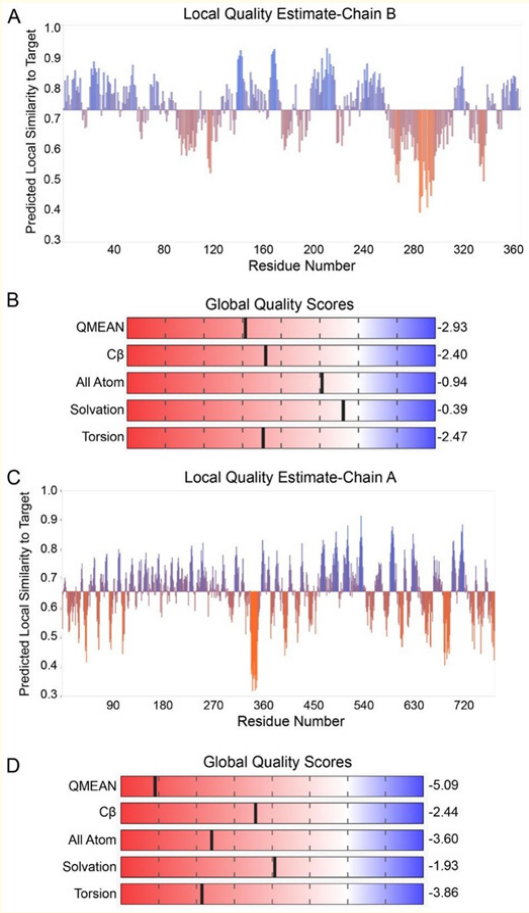

Figure 2: Quality assessment of the modeled *R. solanacearum* XopQ and *N. rustica* Roq1 protein structures using the QMEAN 4.3.1 tool. Evaluation is based on QMEAN scoring functions and global scores in comparison with the experimentally resolved PDB structures. A) Local quality estimation of the XopQ protein, B) Global quality score of the XopQ protein, C) Local quality estimation of the Roq1 protein, and D) Global quality score of the Roq1 protein.

Based on the Ramachandran plot analysis (Figure 3), the *R. solanacearum* XopQ protein model has 90.2% (282) residues in the most favored regions, 8.2 % (26) residues in additionally allowed regions, 0.3% (1) residue in generously allowed regions, and 1.3 % (4) residues in disallowed regions. In comparison, the *N. rustica* Roq1 protein contains 82.4 % (584) residues in the most favored regions, 16.5 % (117) residues in additionally allowed regions, 0.6 % (4) residues in generously allowed regions, and 0.6 % (4) residues in disallowed regions.

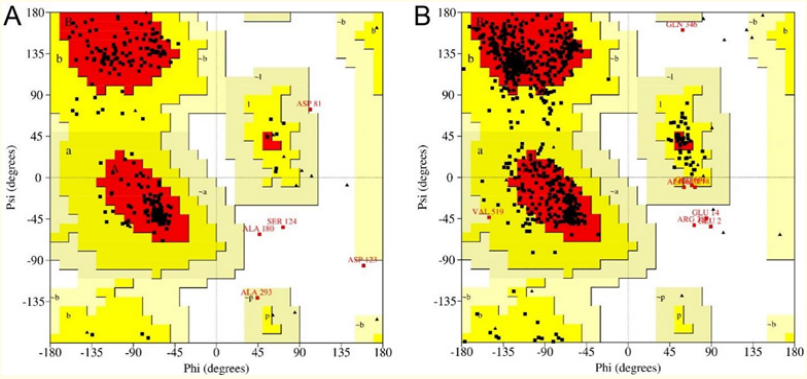

Figure 3: Ramachandran plots analysis of the predicted structures of the *R. solanacearum* XopQ and *N. rustica* Roq1 proteins. The plots depict the distribution of backbone torsion angles (ψ and φ) ranging from -180 ° to +180 °. Different shades of black indicate the favored, allowed, generously allowed, and disallowed regions. A) Ramachandran plot of the *R. solanacearum* XopQ protein, while B) Ramachandran plot of the *N. rustica* Roq1 protein.

Protein-protein molecular docking

The protein-protein interaction complex between the *N. rustica* Roq1 and *R. solanacearum* XopQ was generated using the ZDOCK 3.0.2 server [34], with key residues at the interaction interface highlighted in Figure 4.

Identification and characterization of binding hot spots at protein-protein interface

The binding hot spot residues of the *R. solanacearum* XopQ protein (Table 2) include Trp^{1074}, Asp^{1076}, Ser^{1077}, Trp^{1079}, Tyr^{1169}, Glu^{1172}, Glu^{1174}, Gly^{1175}, Met^{1177}, His^{1178}, His^{1179}, Tyr^{1180}, Ser^{1184}, and Trp^{1187}. For the *N. rustica* Roq1 protein (Table 2), the identified hot spot residues are Asp^{120}, Asp^{180}, Pro^{182}, Thr^{184}, Ser^{185}, Arg^{217}, Leu^{220}, Ala^{243}, Glu^{244}, Leu^{248}, Arg^{277}, Asp^{284}, His^{286}, Tyr^{311}, Ala^{341}, Leu^{345}, Leu^{353}, Ile^{354}, Trp^{361}, Phe^{363}, Phe^{366}, Lys^{394}, and Tyr^{398}.

Comparative molecular dynamics simulation and conformational stability analysis

Molecular dynamics simulations and subsequent trajectory analyses generated several parameters, including Root Mean Square Deviation (RMSD), Root Mean Square Fluctuation (RMSF), structural compactness measured as Radius of Gyration (Rg), Solvent-Accessible Surface Area (SASA), and average number of hydrogen bonds in each frame over time (H bonds). Post-MD simulation stability analysis indicated that the XopQ-Roq1 complex stabilized after 6.15 ns, whereas the *R. solanacearum* XopQ protein alone stabilized after 10.6 ns, and the *N. rustica* Roq1 protein alone required 26.0 ns to reach equilibrium (Figure 5). RMSF analysis showed that the *R. solanacearum* XopQ protein in isolation exhibited fluctuation of 0.7072 nm at the 265^{th} residue, which decreased to 0.261 nm

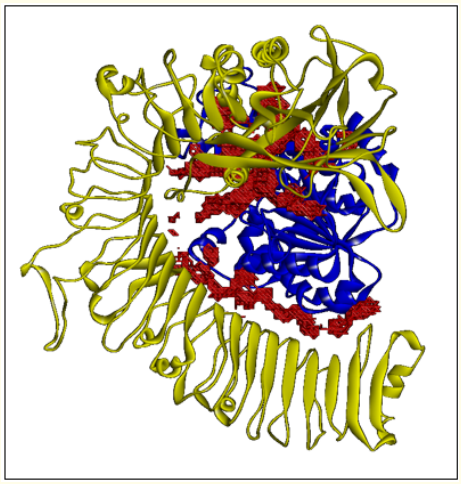

Figure 4: A pictorial representation of an interactive model of the *N. rustica* Roq1 and *R. solanacearum* XopQ proteins. The interacting key residues at the protein-protein interface are shown in the model (black rough outlines). The *N. rustica* Roq1 protein is represented with a white shade, while the *R. solanacearum* XopQ protein is represented with a black shade.

Table 2: Analysis of predicted *R. solanacearum* XopQ and *N. rustica* Roq1 protein structures for interacting residues and binding hot spots using the KFC Server.

Protein Model	Source	Residues Involved in the Interaction
XopQ	*Ralstonia solanacearum*	Trp^{1074}, Asp^{1076}, Ser^{1077}, Trp^{1079}, Tyr^{1169}, Glu^{1172}, Glu^{1174}, Gly^{1175}, Met^{1177}, His^{1178}, His^{1179}, Tyr^{1180}, Ser^{1184}, Trp^{1187}
Roq1	*Nicotiana rustica*	Asp^{120}, Asp^{180}, Pro^{182}, Thr^{184}, Ser^{185}, Arg^{217}, Leu^{220}, Ala^{243}, Glu^{244}, Leu^{248}, Arg^{277}, Asp^{284}, His^{286}, Tyr^{311}, Ala^{341}, Leu^{345}, Leu^{353}, Ile^{354}, Trp^{361}, Phe^{363}, Phe^{366}, Lys^{394}, Tyr^{398}

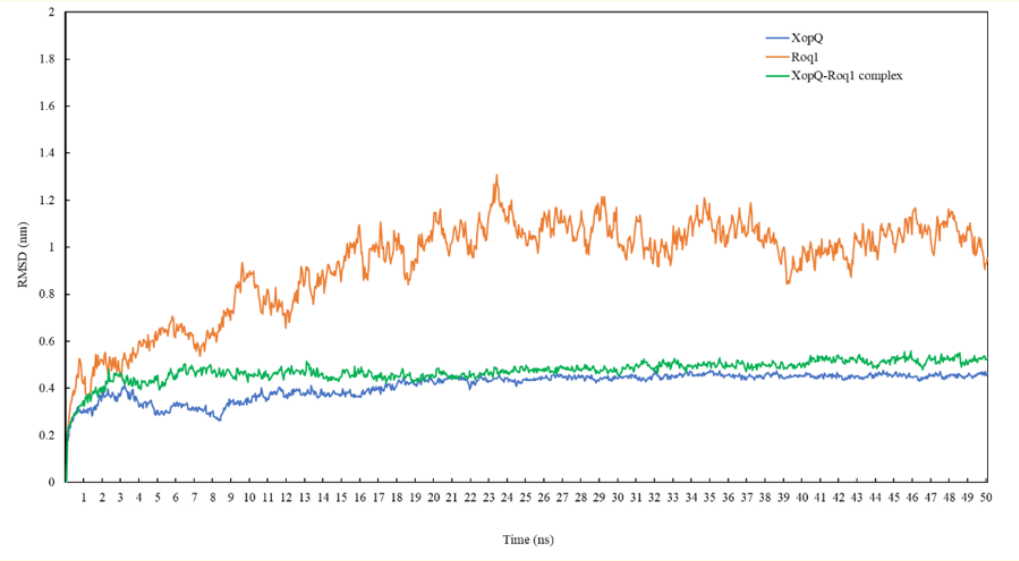

Figure 5: Graphical representation of comparative molecular dynamics simulation analysis of the *R. Solanacearum* XopQ protein, N. rustica Roq1 protein, and the XopQ-Roq1 complex. The plot depicts residue-wise Root Mean Square Deviation (RMSD) values (in nm) calculated over a 50 ns MD simulation using GROMACS.

in the complex (Figure 6), confirming that protein–protein interaction reduces local flexibility and enhances complex stability. Similarly, the *N. rustica* Roq1 displayed a fluctuation of 0.7046 nm in isolation at the 657th residue, which was significantly reduced to 0.1535 nm upon complex formation (Figure 7), further confirming stabilization upon interaction.

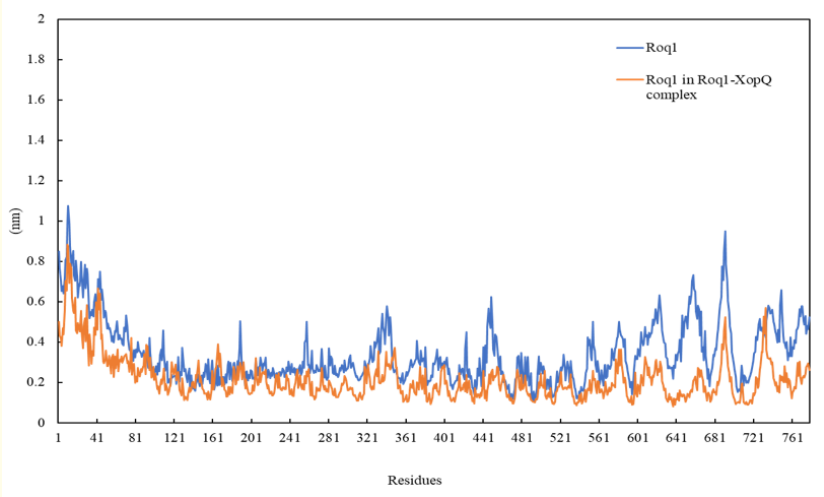

Figure 6: Graphical representation of comparative RMSF values (in nm) of the *N. rustica* XopQ protein in its unbound form and when complexed with the *R. solanacearum* Roq1 protein, as computed from a 50 ns MD simulation using GROMACS.

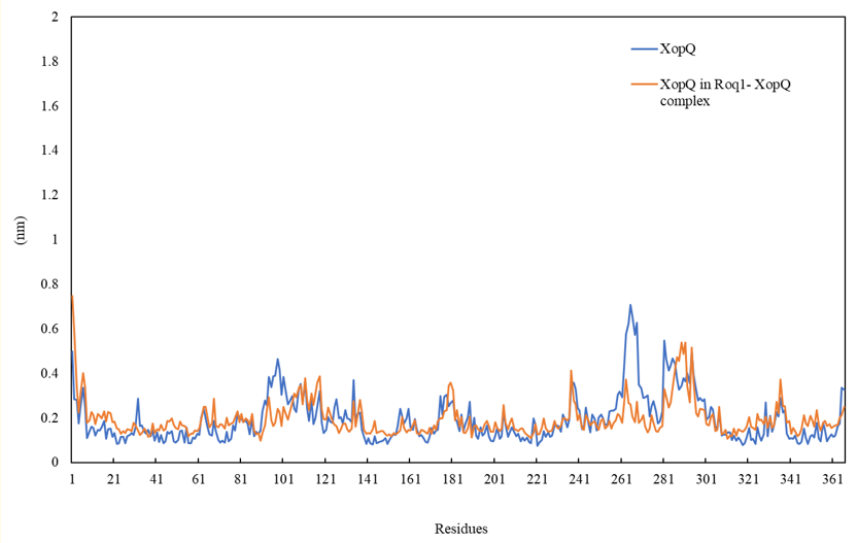

Figure 7: Graphical representation of comparative RMSF values (in nm) of the *R. solanacearum* Roq1 protein in its unbound form and when complexed with the *N. rustica* XopQ protein, as computed from a 50 ns MD simulation using GROMACS.

Discussion

The interaction between plants and pathogens is a dynamic, continuous, and co-evolutionary process. Host plants recognize pathogens through specific molecular patterns, which activate their defense mechanisms. The pathogens, in turn, secrete effector proteins via the Type III secretion system to modulate host immune responses. These effectors act as a modulator of immune responses in the host plants. One such effector, XopQ from *Xanthomonas euvesicatoria*, is highly conserved and widely distributed among various pathogen species, and is known to interact with the Roq1 protein in many Solanaceae species. XopQ is recognized by the NLR superfamily of intracellular immune receptors, among which the Toll/interleukin-1 receptor-NLR is more commonly observed [17].

The lack of experimentally resolved 3D structures of *Nicotiana rustica* Roq1 and *Ralstonia solanacearum* XopQ proteins led us to identify and characterize the interactions between them. Hence, we retrieved the whole genome of *N. rustica* from the NCBI as a whole genome shotgun sequence, and submitted it to FGENESH to deduce the possible amino acid sequence [20]. Physico-chemical characterization revealed that the *N. rustica* Roq1 is a large protein (~151 kDa) rich in charged amino acids, whereas the *R. solanacearum* XopQ protein is smaller (~52.4 kDa) and contains more aliphatic residues.

Homology modeling using the SWISS-MODEL server based on structural templates from both *N. benthamiana* and *X. euvesicatoria* generated reliable 3D structures of both proteins [23]. The models were structurally validated using ERRAT, VERIFY 3D, and PROCHECK tools from the SAVES v6.1 server [24-26], and visualized in BIOVIA Discovery Studio 2021 [29]. CATH database classification was used to classify the target proteins [30]. The CATH results indicate that XopQ belongs to the Ribonucleoside Hydrolase-like homologous superfamily, with an αβ complex architecture (CATH ID: 3.90), and Inosine-uridine Nucleoside N-ribohydrolase topography (CATH ID: 3.90.245). Roq1 belongs to the TIR domain homologous superfamily (CATH ID: 3.40.50.10140), exhibits a 3-layer (αβα) sandwich architecture (CATH ID: 3.40), and a Rossmann fold topography (CATH ID: 3.40.50). Importantly, both proteins fall within the αβ class of proteins (CATH ID: 3).

The QMEAN 4.3.1 tool was used to assess the local and global reliability of the models [31]. InterProScan analysis of the identified *N. rustica* Roq1 amino acid sequence revealed multiple structural domains, motifs, and functional signatures [21]. Roq1 was classified under the disease-resistance protein family (InterPro ID: IPR044974) and the leucine-rich repeat domain superfamily (InterPro ID: IPR032675). Its functional domains included the TIR homology domain (InterPro ID: IPR000157), NB-ARC domain (InterPro ID: IPR002182), and the C-terminal jelly roll/Ig-like domain (C-JID) (InterPro ID: IPR045344). InterProScan annotations indicate its functional roles in signal transduction, defense response, and ADP binding. The *R. solanacearum* XopQ was classified under the ribonucleoside hydrolase-like superfamily (GO:0016799).

Protein-protein molecular docking was performed via the ZDOCK 3.0.2 server [34] to study the interaction between the *N. rustica* Roq1 and *R. solanacearum* XopQ proteins. The Roq1-XopQ interaction complex was further analyzed to identify key interface residues. Binding hot spots at the protein-protein interface were predicted on the basis of structural and physicochemical parameters using the KFC Server [35]. Key residues involved in the molecular interaction between the two proteins were highlighted (Figure 4) and listed (Table 2). The KFC Server predicts the binding hot spots at the interaction interfaces of proteins by identifying the key structural and physicochemical features known to correlate with strong binding affinities based on the already available experimental data. The KFC server analysis identified a total of 14 hotspot residues in Roq1 and 23 residues in XopQ that are involved in stable protein–protein interactions. MD simulation analysis demonstrated that the XopQ-Roq1 complex stabilized after 6.15 ns. The Roq1 protein exhibited greater structural flexibility and instability in its unbound form but showed significant stabilization upon binding to the XopQ effector.

Conclusions

We employed a computational approach to characterize the molecular interaction between the *Nicotiana rustica* Roq1 and *Ralstonia solanacearum* XopQ proteins. A total of 14 amino acid residues from Roq1 and 23 residues from XopQ were found to be actively

involved in protein-protein interaction. Molecular dynamics simulations, including residue-wise Root Mean Square Deviation and Root Mean Square Fluctuation analyses, were performed to assess the conformational stability of the individual target proteins and their complex. The Roq1 protein exhibited greater structural flexibility and instability in its unbound form, but it was significantly reduced upon binding to XopQ, indicating significant stabilization of the complex. This structural transition suggests that Roq1 plays a crucial role in modulating host defense mechanisms. Overall, the findings of the present study provide a basis for deciphering downstream signaling events in plant-pathogen interactions. However, since our findings are derived from *in silico* predictions, additional experimental investigations, including site-directed mutagenesis or binding assays, are essential to confirm the biological significance of these interactions and comprehensively clarify their function in plant-pathogen signaling pathways.

Data Availability

The datasets generated and analyzed during the current study are available in the manuscript itself.

Bibliography

1. AT Thera., *et al*. "Bacterial wilt of Solanaceae caused by Ralstonia solanacearum race 1 biovar 3 in Mali". *Plant Disease* 94 (2010): 372.

2. AC Hayward. "Biology and epidemiology of bacterial wilt caused by Pseudomonas solanacearum". *Annual Review of Phytopathology* 29 (1991): 65-87.

3. S Genin. "Molecular traits controlling host range and adaptation to plants in Ralstonia solanacearum". *New Phytologist* 187 (2010): 920-928.

4. M Katawczik and AL Mila. "Plant age and strain of Ralstonia solanacearum affect the expression of resistance of tobacco cultivars to Granville wilt". *Tobacco Science* 49 (2012): 8-13.

5. D Caldwell., *et al*. "Ralstonia solanacearum differentially colonizes roots of resistant and susceptible tomato plants". *Phytopathology* 107.5 (2017): 528-536.

6. W Röper., *et al*. "Nicotine production by tissue cultures of tobacco as influenced by various culture parameters". *Journal of Plant Physiology* 118.6 (1985): 463-470.

7. A Block., *et al*. "Phytopathogen type III effector weaponry and their plant targets". *Current Opinion in Plant Biology* 11.4 (2008): 396-403.

8. A Schultink., *et al*. "Roq1 mediates recognition of the Xanthomonas and Pseudomonas effector proteins XopQ and HopQ1". *The Plant Journal* 92.4 (2017): 787-795.

9. N Adlung., *et al*. "Non-host resistance induced by the Xanthomonas effector XopQ is widespread within the genus Nicotiana and functionally depends on EDS1". *Frontiers in Plant Science* 7.1796 (2016).

10. V Vyas., *et al*. "Homology modelling—a fast tool for drug discovery: current perspectives". *Indian Journal of Pharmaceutical Sciences* 74.1 (2012): 1.

11. G Launay and T Simonson. "Homology modelling of protein-protein complexes: a simple method and its possibilities and limitations". *BMC Bioinformatics* 9(2008): 427.

12. H Geng., *et al*. "Applications of molecular dynamics simulation in structure prediction of peptides and proteins". *Computational and Structural Biotechnology Journal* 17(2019): 1162-1170.

13. T Boller T and G. Felix. "A renaissance of elicitors: perception of microbe-associated molecular patterns and danger signals by pattern-recognition receptors". *Annual Review of Plant Biology* 60(2009): 379-406.

14. JR Alfano and A. Collmer. "Type III secretion system effector proteins: double agents in bacterial disease and plant defense". *Annual Review of Phytopathology* 42(2004): 385-414.

15. JDG Jones and JL Dangl. "The plant immune system". *Nature* 444.7117 (2006): 323-329.

16. JDG Jones., *et al*. "Intracellular innate immune surveillance devices in plants and animals". *Science* 354.6316 (2016): aaf6395.

17. S Huang., *et al*. "NLR signaling in plants: from resistosomes to second messengers". *Trends in Biochemical Sciences* 48.8 (2023): 776-787.

18. R Martin., *et al*. "Structure of the activated ROQ1 resistosome directly recognizing the pathogen effector XopQ". *Science* 370.6521 (2020): abd9993.

19. CRR Sabbagh., *et al*. "Pangenomic type III effector database of the plant pathogenic Ralstonia spp". *PeerJ* 7 (2019): e7346.

20. V Solovyev., *et al*. "Automatic annotation of eukaryotic genes, pseudogenes and promoters". *Genome Biology* 7.1 (2006): S10.

21. T Paysan-Lafosse., *et al*. "InterPro in 2022". *Nucleic Acids Research* 51.D1 (2022): D418-27.

22. E Gasteiger., *et al*. "Protein identification and analysis tools on the ExPASy server". In: The Proteomics Protocols Handbook. New York: Humana Press; (2005): 571-607.

23. A Waterhouse., *et al*. "SWISS-MODEL: homology modelling of protein structures and complexes". *Nucleic Acids Research* 46.W1 (2018): W296-303.

24. C Colovos and TO Yeates. "Verification of protein structures: patterns of nonbonded atomic interactions". Protein Science 2(9 (1993): 1511-1519.

25. JU Bowie., *et al*. "A method to identify protein sequences that fold into a known three-dimensional structure". *Science* 253.5016 (1991): 164-170.

26. R Laskowski., *et al*. "AQUA and PROCHECK-NMR: programs for checking the quality of protein structures solved by NMR". *Journal of Biomolecular NMR* 8.4 (1996): 477-486.

27. R Shaw., *et al*. "Computational three-dimensional modelling of the β-subunit of follicle-stimulating hormone in stinging catfish (Heteropneustes fossilis)". *Acta Scientific Veterinary Sciences* 6.10 (2024): 52-61.

28. BIOVIA, Dassault Systèmes. "BIOVIA Discovery Studio software". San Diego: Dassault Systèmes; (2021).

29. I Sillitoe., *et al*. "CATH: increased structural coverage of functional space". *Nucleic Acids Research* 49.D1 (2021): D266-273.

30. G Studer., *et al*. "QMEANDisCo—distance constraints applied on model quality estimation". *Bioinformatics* 36(6 (2020): 1765-1771.

31. D Chowdhury., *et al*. "Peptides on a rescue mission against the hazardous cidal chemicals used in Eastern Indian Agriculture: An in-silico approach based on field survey in 2020". *Environmental Health Engineering and Management Journal* 8.2 (2021): 107-122.

32. I Singh., *et al*. "Evaluating the relative efficacy of synthetic and natural drugs in endometriosis adopting molecular modelling approach". *Journal of Endocrinology and Reproduction* (2023): 297-291.

33. BG Pierce., *et al*. "Accelerating protein docking in ZDOCK using an advanced 3D convolution library". *PLoS One* 6(9 (2011): e24657.

34. X Zhu and JC Mitchell. "KFC2: a knowledge-based hot spot prediction method based on interface solvation, atomic density, and plasticity features". *Proteins* 79.9 (2011): 2671-2683.

35. SJ Darnell., *et al*. "An automated decision-tree approach to predicting protein interaction hot spots". *Proteins* 68.4 (2007): 813-823.

36. MJ Abraham., *et al*. "GROMACS: High performance molecular simulations through multilevel parallelism from laptops to supercomputers". *SoftwareX* 1-2 (2015): 19-25.